*Exploration Geophysics (2006) **37**, 372–378*

Sources of along-strike variation in magnetic anomalies related to intrasedimentary faults: A case study from the Rio Grande Rift, USA

V.J.S. Grauch Mark R. Hudson Scott A. Minor Jonathan Saul Caine

Key Words: magnetic anomalies, intrasedimentary faults, sedimentary basins, aeromagnetic surveys, magnetic sources of faulted layers.

ABSTRACT

Normal faults within sedimentary basins are commonly associated with subtle linear features in high-resolution, total magnetic intensity (TMI) data. Many of these anomalies arise from the tectonic juxtaposition of sedimentary units of differing magnetic properties. In detail, the anomalies can be quite variable in character, even along the strike of individual faults. To understand this variability, we examine the well-exposed San Ysidro Fault in the central Rio Grande Rift, USA, using detailed magnetic-property measurements, geophysical models based on geology, and Euler analysis. We find that along-strike anomaly variability arises mainly from (1) multi-levelled magnetic contrasts at the fault that are variably sampled by uneven levels of erosion, and to a lesser extent from (2) magnetic susceptibilities that vary along strike within individual units, and (3) variable throw and dip of the fault that produces differences in the extents to which contrasting units are in contact. The multi-levelled magnetic contrasts arise from the juxtaposition of different strata across the fault at discrete depths. Locations of magnetic sources along the fault estimated from Euler analysis of the TMI data reflect the variations in depths to the shallowest sources along strike. Variations in clustering of the Euler solutions suggest that the sources have variable geometry (structural index). The results at the San Ysidro Fault demonstrate the important and complex role of multi-levelled magnetic sources in understanding anomalies associated with faulted geologic layers in general. The potential for multiple sources suggests that the use of simple model geometries to represent faults may not always be appropriate.

INTRODUCTION

Faults within sedimentary basins are commonly associated with subtle linear anomalies in high-resolution total magnetic intensity (TMI) data. The anomalies may arise from contrasts caused by tectonic juxtaposition of sedimentary layers with differing magnetic properties or from secondary magnetisation produced by geochemical activity along the fault zone (Gunn, 1997).

Tectonic juxtaposition can plausibly explain all of the anomalies related to intrasedimentary faults observed in the Albuquerque Basin (Grauch et al., 2001), a large sediment-filled basin that composes the central part of the Rio Grande Rift in northern New Mexico, USA (Fig. 1). The anomalies range in amplitude from 2 to 40 nT (for data continued to 100 m above ground), display anastomosing and en echelon patterns in map view, and show a range of shapes and amplitudes in profile view. The observed variation in anomaly shape between faults can be explained by differences in how layers of differing thickness are juxtaposed at the fault (Grauch et al., 2000).

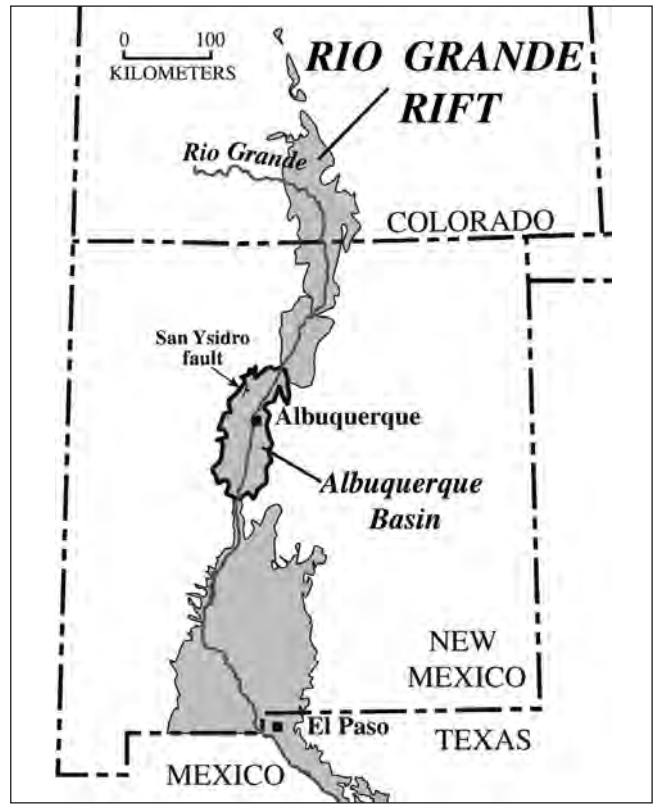

Fig. 1. Location of the Albuquerque Basin within the Rio Grande Rift, southwestern USA, and general location of the San Ysidro Fault.

More difficult to explain are the differences in anomaly shape that are observed along the strike of a single fault. Significant differences in amplitude, including near lack of expression in some places, may reasonably be explained by the high variability of magnetic properties of sediments. However, the variations in anomaly width and steepness of gradients are harder to explain because they signal differences in the locations or types of the magnetic sources.

Detailed studies identifying geologic sources of magnetic anomalies in sedimentary environments are rare in the literature (Mushayandebvu and Davies, 2006). To better understand along-strike anomaly variability, we undertook such a detailed study at the San Ysidro Fault, an exceptionally well-exposed fault in the central Rio Grande Rift, USA (Fig. 1). It is a major rift-related intrasedimentary fault serendipitously situated within badlands topography, so that varying structural depths of the fault can be examined along strike (Fig. 2a). A 10–20 nT linear anomaly generally follows most of the mapped extent of the fault, with

U. S. Geological Survey
MS 964, Federal Center,
Denver, Colorado, USA 80225-0046
Phone: +1 303 236 1393
Facsimile: +1 303 236 1425
Email: tien@usgs.gov

Presented at the 18th ASEG Geophysical Conference & Exhibition (AESC2006), July, 2006. Revised manuscript received 5 October, 2006.

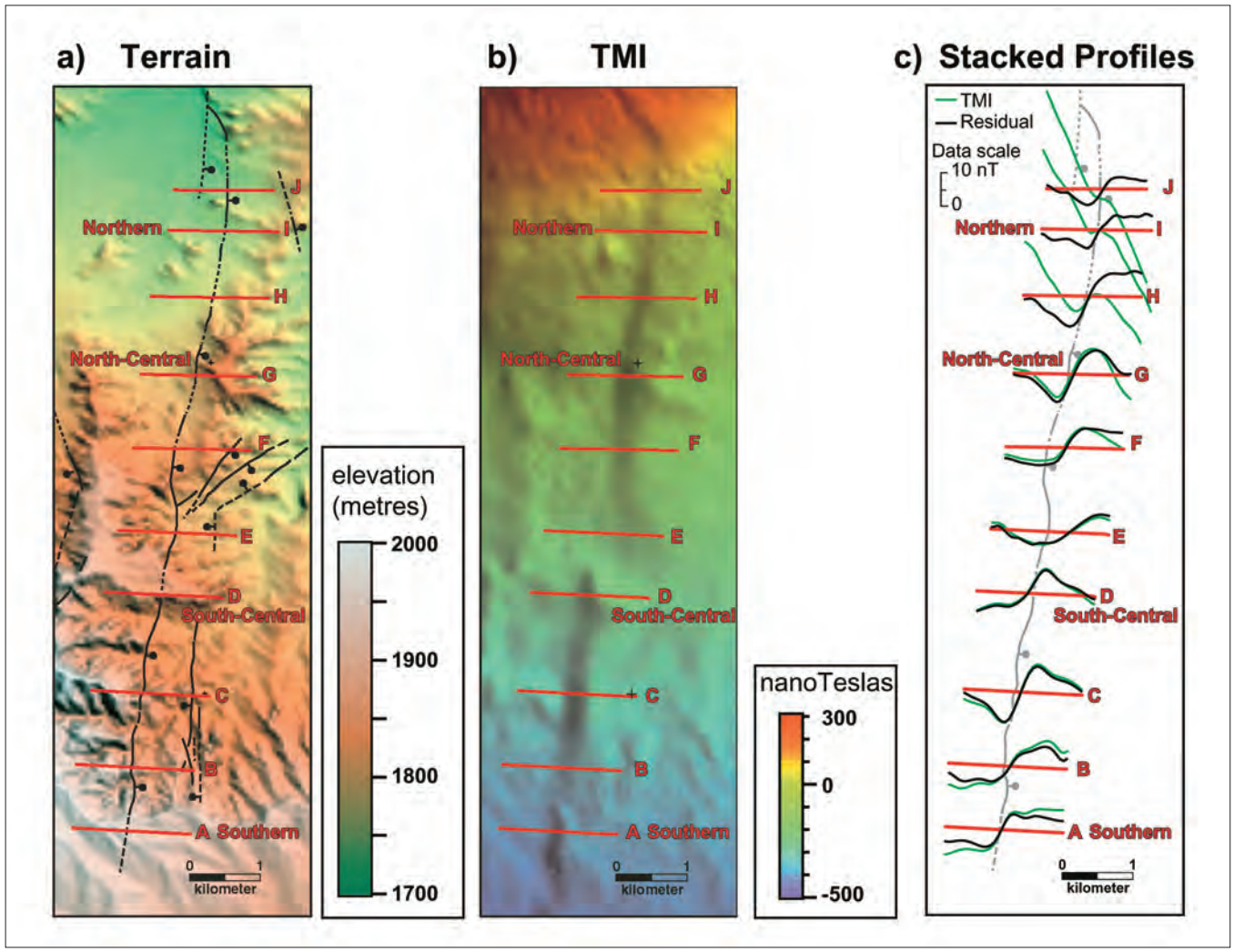

Fig. 2. Location and magnetic expression of the San Ysidro Fault along strike showing the locations of selected profiles (red lines). Terrain (a), represented by U.S. Geological Survey 30-m digital raster elevation data (illuminated from the east), is overlain by the through-going San Ysidro and related minor faults as mapped by Koning et al. (1998). Erosion and stratigraphic dip expose increasingly deeper levels of the fault from south to north. Total magnetic intensity (TMI) data analytically continued to a surface 100 m above ground are shown in a colour shaded-relief image illuminated from the east (b). TMI and residual data are shown as stacked profiles in (c) after removal of mean values for each profile. Residual TMI data for profiles A, D, G, and I are compared to forward model curves in Figure 5.

amplitudes near zero locally and variations in anomaly shape along strike (Fig. 2b and 2c). This study is one of several investigations by the authors to explore relations between the hydrogeology, structural geology, magnetic properties, and aeromagnetic expression of intrasedimentary faults in the central Rio Grande Rift. Reports summarising the other investigations are being prepared separately.

The detailed study of magnetic sources involved the development of several magnetic profile models of observed airborne data, each based solely on mapped geology (Koning et al., 1998; modified by Hudson, Caine, and Minor), structural observations (Minor and Caine), and extensive magnetic-susceptibility measurements of exposed units (Hudson). The models, along with depth estimates provided by Euler analysis of residual TMI data, demonstrate that multiple magnetic contrasts occur at different depths along the fault. The case study at the San Ysidro Fault illustrates the important role that multiple contrasts may play in understanding anomalies associated with faulted geologic layers in general.

GEOLOGY AND MAGNETIC PROPERTIES

The San Ysidro Fault is a major rift-related normal fault located near the north-western margin of the Albuquerque Basin, New Mexico (Fig. 1). More than 1000 m of sedimentary section is exposed and offset as much as 670 m across this northerly-striking, down-to-the-east fault. The faulted sedimentary section consists of ~1000 m of poorly to moderately lithified, clastic sedimentary units deposited during development of the Rio Grande Rift, underlain by 1–3 km of pre-rift, primarily clastic sedimentary rocks (Fig. 3). The syn-rift Santa Fe Group includes ~600 m of mainly eolian sandstones of the Zia Formation, overlain by ~400 m of Arroyo Ojito Formation, composed primarily of poorly consolidated, fluvial sands and gravels (Connell et al., 1999; Connell, 2004).

The Zia and Arroyo Ojito Formations are each further divided into three members. The Zia Formation of the lower Santa Fe Group is composed of the Piedra Parada (Tzp), Chamisa Mesa (Tzc) and Cerro Conejo (Tzcc) Members. All three members are consistently dominated by medium-grain, well-sorted sands and sandstone, despite differences in depositional environment. The Arroyo Ojito Formation of the upper Santa Fe Group is composed of the Navajo Draw (Ton), Loma Barbon (Tob), and Ceja (QToc) Members. All three members have wide variability in sediment grain size, although gravel is more dominant higher in the section (Connell, 2004).

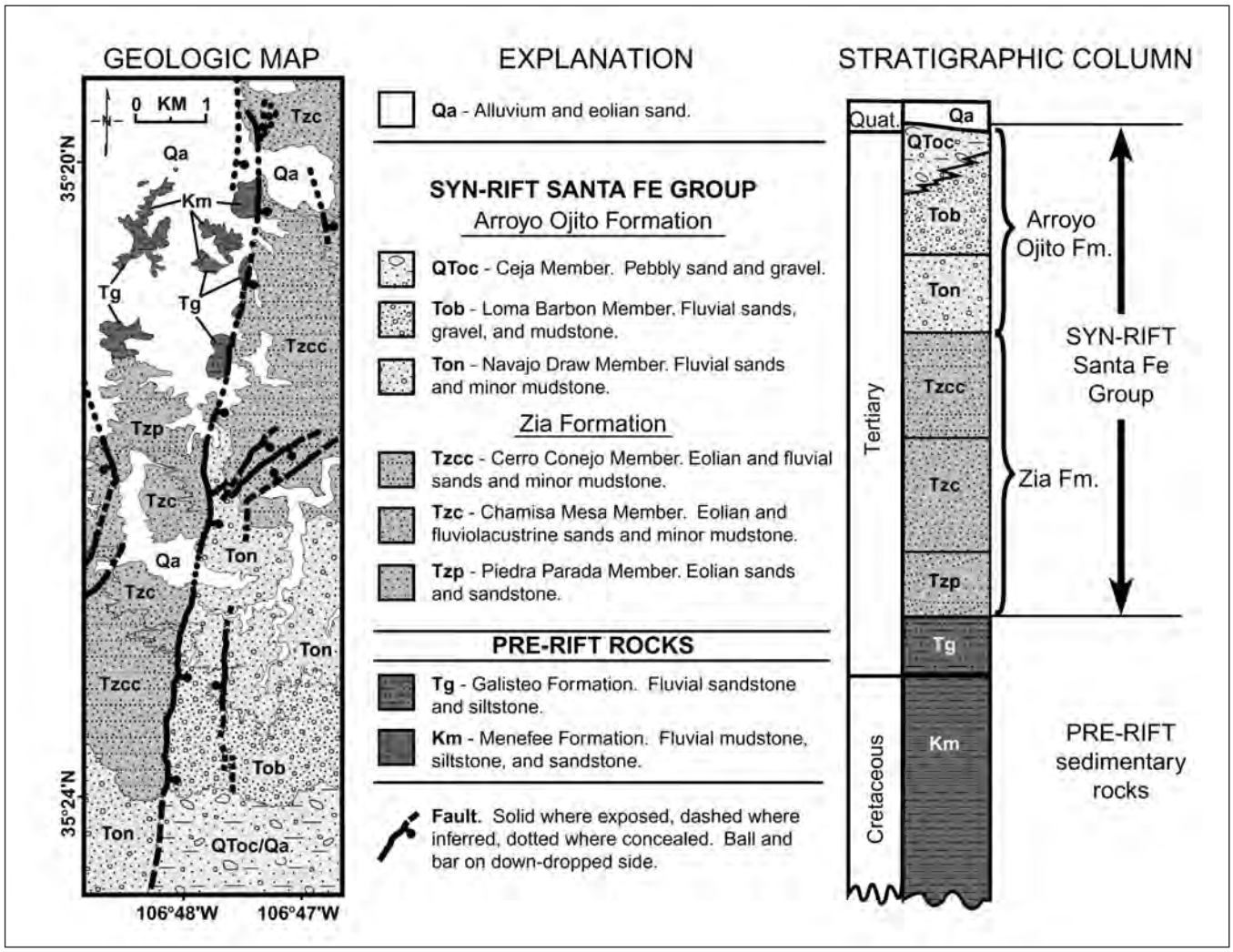

Fig. 3. Geologic map of the area surrounding the San Ysidro Fault and description of stratigraphic units, modified from Koning et al. (1998) and Connell et al. (1999).

Exposed pre-rift sedimentary rocks consist of clastic sedimentary rocks of the Upper Cretaceous Menefee Formation (Km) unconformably overlain by Eocene Galisteo (Tg) Formation (Fig. 3). Regionally, the Menefee Formation is near the top of a thick (~3 km) Phanerozoic sedimentary sequence that overlies Precambrian basement (Russell and Snelson, 1994). However, this sequence was variably uplifted and eroded throughout the region during several Phanerozoic tectonic events, as evidenced by a basement-cored uplift just 10 km to the northwest of the study area. The red-bed sandstone-dominated Galisteo Formation accumulated as sediments were shed from adjacent uplifts towards the end of one of the later orogenies (Cather, 2004).

The San Ysidro fault zone averages about 50 m in width and is variably cemented with carbonate. Fault dip ranges from 55° to 75°. Several minor faults strike parallel or obliquely with respect to the main fault (Fig. 3). In the central part of the study area, the geometry of the oblique faulting at depth is poorly understood.

Magnetic susceptibility measurements from 310 sites, mostly measured on both sides of the San Ysidro Fault, were used to characterise the magnetisation of members of the Arroyo Ojito and Zia Formations (Fig. 4; Hudson et al., 2001; Hudson et al., 2006). The quantity of detrital magnetite is the predominant control on the magnetic susceptibility variations within the Santa Group sediments (Hudson et al., 2006). Members of the Arroyo Ojito Formation show variable magnetic susceptibilities, with a typical range (determined by the 25th and 75th percentiles of the populations) of $0.9–4.3 \times 10^{-3}$ (SI). An exception is the lowermost 30–40 m of the Navajo Draw Member (Ton), which has a typical range of $4.3–8.3 \times 10^{-4}$ (SI) (Fig. 4). The higher susceptibility values of the Arroyo Ojito Formation generally correspond to coarser sediment grain size, with coarse sands and gravels of the Ceja Member (QToc) exhibiting the highest values (Fig. 4; Hudson et al., 2006). Members of the Zia Formation show less variation in magnetic susceptibility and less correlation with grain size compared to those of the Arroyo Ojito Formation. Susceptibility values for the Zia Formation have a typical range of $0.7–1.4 \times 10^{-3}$(SI).

The pre-rift rocks display magnetic susceptibilities that are generally an order of magnitude less than the syn-rift units, ranging from $0.7–2.0 \times 10^{-4}$ (Fig. 4). A general down-section decrease in magnetic susceptibility in the Galisteo Formation is observed, but difficult to characterise statistically.

Slight decreases in the median values of magnetic susceptibility are associated with strongly cemented portions of the fault zone, but still fall within the typical ranges for individual stratigraphic units. Magnetite was likely oxidised by paleo-ground-water flow that was concentrated at the fault zone (Hudson et al., 2006). Insignificant variations in magnetic properties across cemented zones were also observed at another rift fault, about 15 km to the northeast of the study area (Grauch et al., 2001).

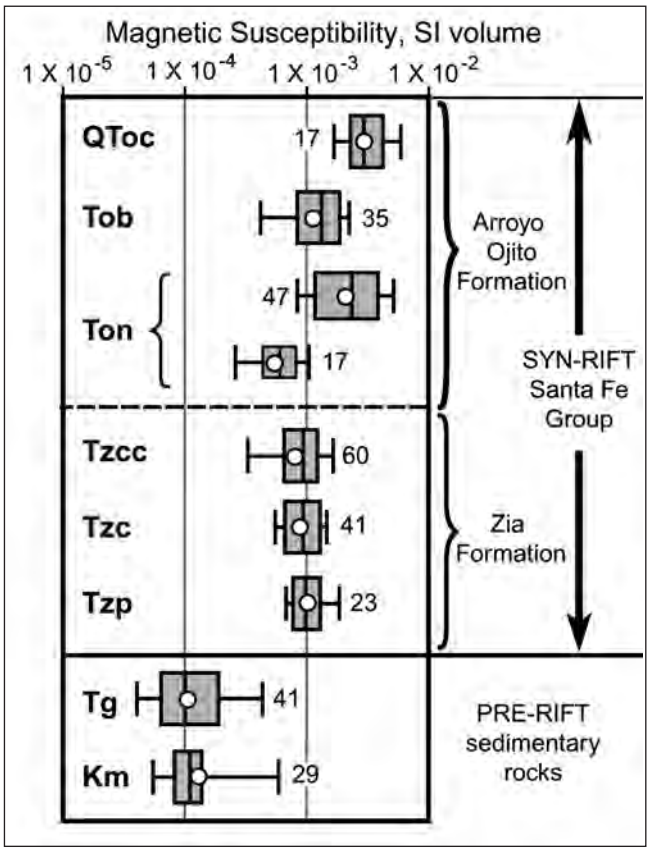

Fig. 4. Statistical characterisation of magnetic susceptibilities for stratigraphic units cut by the San Ysidro Fault. Unit codes are described in Figure 3. The box and whisker plots show geometric mean (open circle), median (vertical line), and ranges of the population's 25th and 75th (grey boxes) and 10th and 90th (whiskers) percentiles. The number of field sites is listed next to each box and whisker plot. Two box and whisker plots are shown for the Navajo Draw Member (Ton) because the values for the basal 30–40 m of the unit are significantly lower than is inferred for the upper ~180 m of the unit.

MAGNETIC MODELS

TMI data over the San Ysidro Fault are available from a fixed-wing survey flown along east-west lines spaced 150 m apart at a nominal terrain clearance of 150 m (U.S. Geological Survey et al., 1999). Data from the survey were gridded at a 50-m interval then analytically continued to a consistent 100 m above ground (Fig. 2b; Sweeney et al., 2002). The 1:1 ratio of line spacing to terrain clearance properly samples the magnetic field for analysis of 3D sources at the ground surface (Reid, 1980), allowing downward continuation to increase signal without introducing aliasing artefacts. Whereas some high-frequency information is lost along flight lines, resolution in both along-track and cross-track directions are comparable. Thus, we can optimally study sources that do not have a true north-south strike, such as the San Ysidro Fault of this study. Additionally, a regional field digitised from TMI contours was removed from the gridded, analytically continued TMI data before the profiles were extracted for modelling. Data extracted from the TMI and residual grids are compared for ten profiles crossing the San Ysidro Fault in Figure 2c. The northern profiles (H–J) show the greatest influence of a regional gradient.

To test whether the magnetic-susceptibility characterisations of the stratigraphic units were truly representative of the magnetic sources at the San Ysidro Fault, we developed forward magnetic models (Fig. 5) for four of the ten profiles across the fault (A, D, G, and I, located on Fig. 2). The models were constructed by assigning the geometric means of the measured magnetic susceptibility values to the corresponding layers in geologically constructed cross sections, totally independent of the TMI data. The magnetic effects of these models (calculated curves) were computed using a 2D Talwani polygonal algorithm and plotted for comparison to the residual TMI data (observed curves). To facilitate discussion, the geologic units that are juxtaposed vertically along the fault and the corresponding magnetic-susceptibility contrasts are indicated to the right of each model (Fig. 5). Positive or negative contrasts at the fault indicate that the more magnetic of the juxtaposed units and its consequent anomaly high are on the east or west side of the fault, respectively.

The model for the southernmost profile A (Fig. 5a) corresponds to the greatest thickness of sedimentary section juxtaposed at the fault. Note that the geometric means assigned to the Navajo Draw Member (Ton) differ between the hanging-wall and footwall blocks, corresponding to values of the thick upper and thin lower portions of the member, respectively. The good fit of the model lends credibility to the magnetic-susceptibility characterisation of the individual units.

The profile A model and corresponding bar graph of magnetic-susceptibility contrasts (Fig. 5a) imply that the observed anomaly is caused primarily by the sum of the effects of several positive magnetic contrasts at the fault at different depths. Negative magnetic contrasts are generally weaker or less extensive compared to the positive ones, explaining why the observed anomaly has a high on the east rather than the west side of the fault. The shallowest, and therefore most influential, positive contrasts range from about $0.3–1 \times 10^{-3}$ SI and extend 350 m down from the surface. Negative contrasts below these are mostly less ($\sim 2 \times 10^{-4}$ SI) and extend for 250 m vertically. The strong negative contrast at the base of the Navajo Draw (lower Ton against Tzc) likely has little influence owing to its depth and limited vertical extent. Further below, positive contrasts generally are on the order of 1×10^{-3} SI and extend 400 m vertically. These lowest positive contrasts represent a consistent, deep contribution to the anomaly high on the east side of the fault. Below these, magnetic contrasts are considerably less than 1×10^{-5} SI, which have negligible contribution to the overall anomaly.

Compared to the southernmost profile, the south-central profile D (Fig. 5b) crosses the fault at a lower structural level of the juxtaposed section, and fault dip is shallower (56° rather than 70°). Assigning the same magnetic susceptibility values to the model units as in the southernmost profile, the forward model fits only to a first order; misfits are apparent on both ends of the profile. The most significant misfit on the eastern end can be explained by an observed decrease in grain size and in corresponding susceptibility of the shallow part of the Navajo Draw Member (Ton) away from the fault zone in this area. For simplicity, this level of detail was not included in the model. On the other hand, the good fit over the fault zone suggests that the main sources of the anomaly are positive magnetic contrasts at discrete shallow and deep levels, separated by less significant negative contrasts. The shallower fault dip and greater erosion at this site compared to that of the southernmost profile produces differences in the vertical extent and depth of the positive versus negative contrasts. The overall result is a greater influence of positive contrasts to the anomaly high on the east side of the fault and thus a slightly higher anomaly amplitude (~12 versus 10 nT).

Erosion has completely removed the Arroyo Ojito Formation in the areas of the two northern profiles (Fig. 5c and 5d), so that only the Zia Formation is juxtaposed against pre-rift rocks. The strong positive contrasts that are at deeper levels in the southern profiles are present at the surface in both northern profiles. The

sources of the anomaly for the northernmost profile I (Fig. 5d) can be generally attributed to these positive contrasts because the forward model has a fairly good fit. In contrast, the computed curve for the north-central model G (Fig. 5c) has only a fair fit to the observed data, despite the seemingly simpler geology and greater consistency of magnetic properties expected in comparison to the southern profiles. Additional buried magnetic sources on both sides of the fault at depth seem to be required to explain the misfits of this model. Possible scenarios include indeterminate geologic complexities or interference from neighbouring regional sources that have not been removed adequately.

EULER ANALYSIS

To further assess whether multiple magnetic sources are distributed at different depths along strike of the San Ysidro Fault, we used Euler deconvolution to estimate source locations in three dimensions. Although many other techniques are available for this type of depth analysis, our purpose was not to investigate the methodology. A standard Euler technique (Reid et al., 1990) was applied to the gridded residual TMI data using a window size of 500×500 m. Application of Euler analysis to the residual TMI grid rather than to the original located data ensures that the results are not overwhelmed by high-frequency signal caused by local lithologic variations that are difficult to characterise. A disadvantage is the assumption that the anomaly of interest is always well defined within a 10×10 window. Solutions were rejected if their errors in the least-squares inversion were greater than 10% of the depth, if they were located more than 300 metres from the mapped fault, or if they were otherwise considered unrelated to the San Ysidro Fault by inspection.

An important consideration for Euler analysis is the initial choice of structural index. The structural index describes the rate of fall-off of the magnetic field, which is related to the shape of the source body. An idealised normal fault, having a single magnetic contrast at a fault plane that extends to great depth, should correspond to a structural index of 0. An index between 0 and 1 may be best for a fault where the magnetic contrast has finite depth extent, and an index of 2 can be appropriate for faulted thin beds (Reid, 2003). Solutions obtained from the most appropriate structural index for a fault are normally recognised by how well they cluster in a line. After various trials for the study area, no single structural index gave results that were well clustered everywhere. However, in order to relegate discussions regarding methodology to future work, we show the solutions using a single structural index of 0.5 (Fig. 6), which gave the most solution clusters along the fault. An exception is the area near Profile C, where solutions using a structural index of 0.5 are particularly poorly clustered. For this area only, solutions using structural index of 2 are shown as well, which, curiously, display the best clustering of all structural indices tested.

To better compare the Euler solutions to the models, the schematic columns illustrating the juxtaposed units for each model (Fig. 5) are plotted at the correct northing locations below the fault trace in Figure 6, with additional schematic columns for profiles E and H. Correlation lines, which schematically track the magnetic-contrast interfaces between the columns, surround coloured areas, where warm and cool colours represent positive and negative contrasts, respectively (Fig. 6).

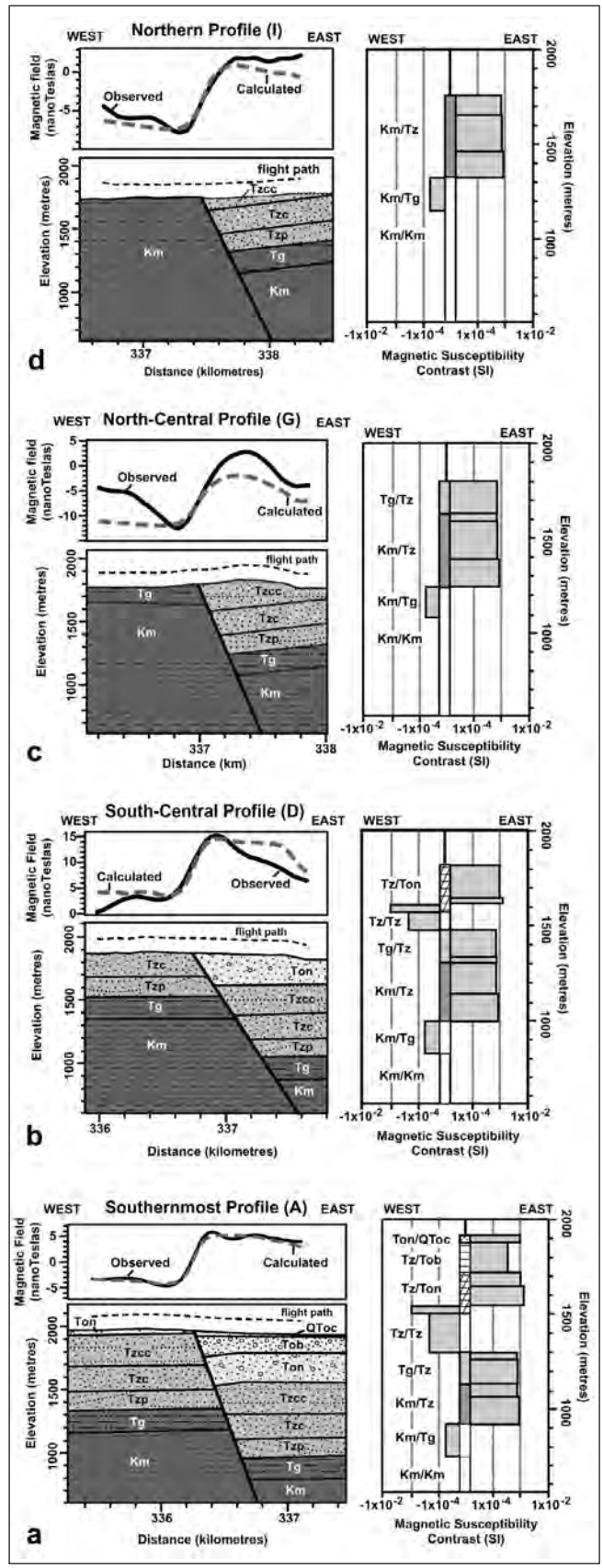

Fig. 5. Forward magnetic models for profiles A (a), D (b), G (c) and I (d), located on Figure 2. The models were constructed from geologic cross-sections and the geometric means of measured magnetic-susceptibilities for each unit, totally independent of the TMI data. The display follows the scheme of Figure 3. Observed (residual TMI data) and calculated magnetic curves (using a Talwani algorithm) are compared. To the right of each model, the geologic units juxtaposed at different levels of the fault are coded (e.g., Tz/Ton) and illustrated by patterns in the central column, the top of which is located at ground surface. The shaded bar graphs show the amount of magnetic-susceptibility contrast (difference between the geometric means of the juxtaposed units). A bar to the right (positive contrast) or a bar to the left (negative contrast) indicates the more magnetic unit is on the east or west side of the fault, respectively.

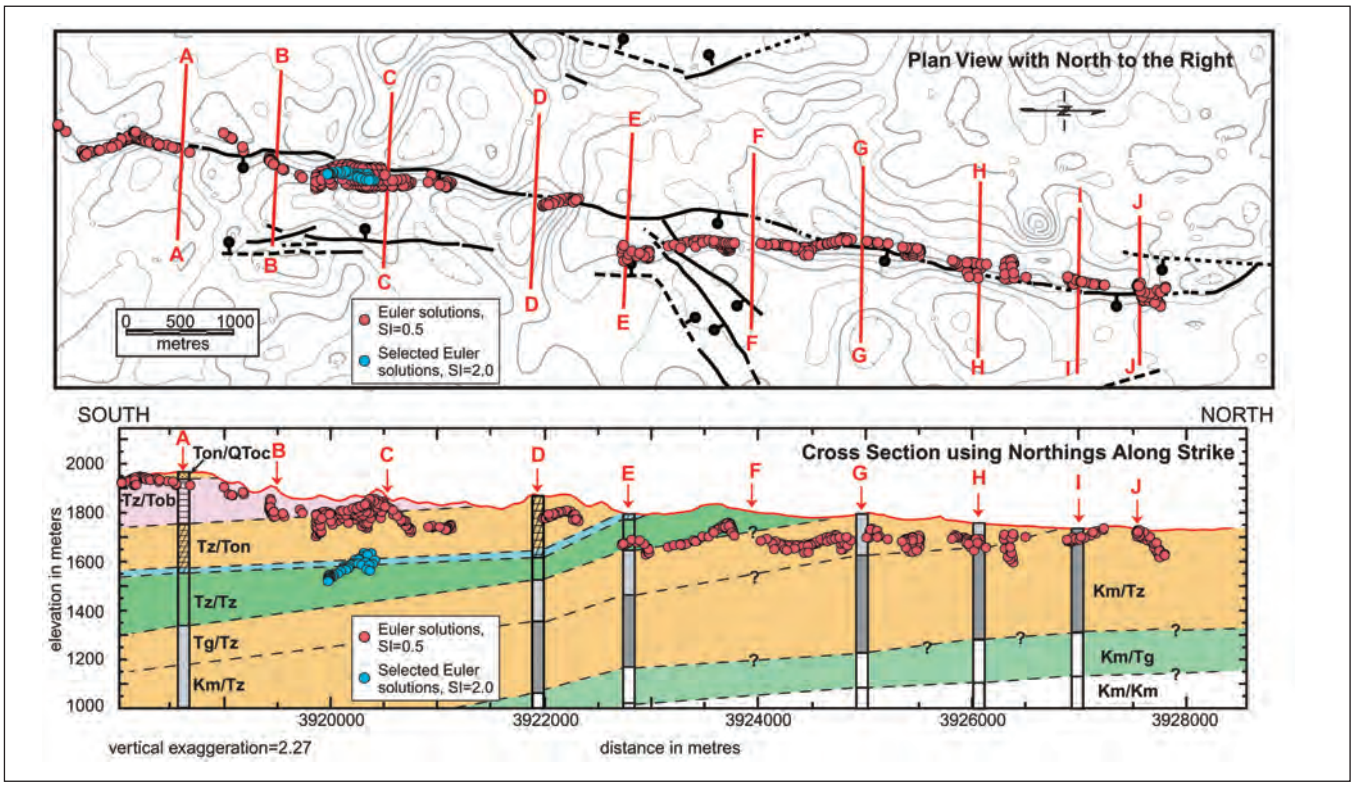

Fig. 6. Results of Euler deconvolution compared to the magnetic-susceptibility contrasts of the forward models. Solution locations using a structural index (SI) of 0.5 (red circles) are plotted in plan view (above) over contours of the residual TMI and in cross section (below) using the northings and elevations of the locations along strike. Solutions for SI=2 (blue circles) are shown only near Profile C. Schematic columns of juxtaposed units are from Figure 5 with additional columns for profiles E and H. Correlation lines drawn between the columns are queried where geology and magnetic interpretation are uncertain. Magnetic-susceptibility contrasts (Fig. 5) are colour coded as follows: orange and pink indicate positive contrasts of ~1×10^{-3} and 3.5×10^{-4} SI, respectively; blue and green indicate negative contrasts of ~1×10^{-3} and less than 2×10^{-4} SI, respectively; white indicates no contrast.

As predicted from the forward models, the Euler solutions locate different sources at different depths along strike of the fault (Fig. 6). At the southern end of the fault (south of profile A), the solutions correspond to the shallowest positive contrast between the Ceja and lower Navajo Draw Members (Ton/QToc). To the north, where the Ceja Member is missing (from south of B to north of D), solutions locate sources at a variety of depths. A structural index of 2 (blue circles) rather than 0.5 is required to obtain well clustered solutions in the area of Profile C, suggesting that source type is variable as well as source depth. These inconsistencies may be explained by the inherent variability of the magnetic susceptibilities of the Arroyo Ojito Formation in contrast to the more consistent values of the Zia Formation. Where all but the weakly magnetic, basal portion of the Arroyo Ojito Formation is missing in the section (from profile E north), the Euler solutions are well clustered and appear to generally follow the gentle stratigraphic dips that bring beds to the surface on the north. At profile E, the near-zero anomaly amplitude over the fault trace is consistent with the lack of magnetic contrast inferred from measured magnetic susceptibilities of juxtaposed units near the surface. North of profile F, the solutions seem to track a magnetic contrast at lower levels than expected, toward the base of the juxtaposition of the Galisteo against Zia Formations (Tg/Tz). The deeper solutions may result from greater contrast caused by the down-section decrease in magnetic susceptibilities of the Galisteo Formation (noted above), from inaccuracies in the depth analysis, or from the effects of unidentified magnetic sources in the Zia Formation on the west side of the fault.

The difference in the Euler results between the southern and northern areas of the fault is most pronounced between profiles D and E. Solutions just north of profile D are fairly well clustered along strike and occur at about 1800 m elevation, located within the section that juxtaposes members of the Zia Formation against the Navajo Draw Member of the Arroyo Ojito Formation (Tz/Ton on Figs. 5b and 6). In contrast, solutions at profile E are clustered at about 1650–1700 m elevation along a magnetic gradient that is located about 300 m east of the fault trace, out of the strike plane. The Euler solutions follow this magnetic gradient until it intersects the trace of the San Ysidro Fault, between profiles F and G, displaying another apparent 100–200 m drop in elevation from south to north across profile F (Fig. 6). If the magnetic gradient represents magnetic contrasts at a dipping San Ysidro Fault at depth, the solution locations imply a fault dip of about 45°, a much shallower dip than measured at the surface or predicted at depth from geologic considerations. This conflicting evidence, along with the mismatches of the model at profile G (Fig. 5c), and an apparent spatial relation between the magnetic gradient and the cross-faulting between profiles E and F (Fig. 6), all support the idea of additional, unidentified magnetic source(s) at depth in the central and northern parts of the study area.

CONCLUSIONS

The sources of along-strike anomaly variability at the San Ysidro Fault are primarily (1) multi-levelled magnetic contrasts that are observed at different depths along strike as a result of uneven erosion and dipping strata, and to a lesser extent from (2) magnetic properties that vary along strike within individual units, and (3) variable fault throw and dip that produce differences in the extents to which contrasting units are in contact at the fault.

Exposure to different levels of the fault zone has the greatest influence on along-strike anomaly variability at the San Ysidro

Fault due to multiple, discrete magnetic contrasts at depth. Positive magnetic-susceptibility contrasts, which produce highs on the east (hanging-wall) side of the fault, are up to an order of magnitude stronger and more vertically extensive than negative contrasts, which produce highs on the west (footwall) side of the fault. Strong positive contrasts of about 1×10^{-3} SI extend from 50–500 m vertically. They represent three distinct sources with finite thicknesses, separated by a weaker (0.3×10^{-3} SI) positive contrast and two negative contrasts at depth. Negative contrasts are generally less than 2×10^{-4} SI and extend from 150–200 m vertically. One negative contrast is about 1×10^{-3} SI but spans only 30–40 m vertically.

The anomalies along the fault primarily reflect which of the multiple magnetic contrasts have been brought near the surface by stratal dip and erosion. The differences in depth and presence of these multiple sources along strike are reflected in the locations of Euler solutions derived from residual TMI data. Poorly to well clustered solutions at variable depths indicate that the magnetic sources cannot be adequately represented by a single source type (structural index). Inconsistent solution depths within sections along strike that juxtapose the same geologic units suggest that some difference in anomaly shape is due to variability of magnetic susceptibility within individual units.

Some of the multiple magnetic contrasts vary in magnitude and vertical extent along strike, as a consequence of variable fault dip and throw that create differences in the extent to which units are juxtaposed. These variations primarily alter anomaly amplitude. Although Euler solutions are significantly offset from the fault trace in the central part of the study area, geologic evidence suggests this is not due to the dip of the fault. The complexities required to explain the discrepancy remain unresolved.

The results at the San Ysidro Fault imply that multi-levelled magnetic sources may be common at faults offsetting sedimentary strata or other layered geology, such as basalt flows. The potential for multiple sources suggests that the use of simple model geometries to represent faults may not always be appropriate. Results of magnetic depth analysis that give irregular results along strike or that are inconsistent with expected depths may signal the presence of multiple sources. This recognition should aid in the geologic interpretation of linear magnetic anomalies in a variety of extensional environments. Moreover, the detailed magnetic-susceptibility characterisation of units juxtaposed at the San Ysidro Fault should provide a useful case history for future investigations of magnetic interpretation techniques.

ACKNOWLEDGMENTS

We thank Jeff Phillips, Rick Saltus, Pierre Keating, and an anonymous reviewer for their helpful suggestions.

REFERENCES

Cather, S.M., 2004, Laramide orogeny in central and northern New Mexico and southern Colorado: in Mack, G.H., and Giles, K.A., (eds.), *The Geology of New Mexico, A Geologic History*: New Mexico Geological Society, 203–248.

Connell, S.D., Koning, D.J., and Cather, S.M., 1999, Revisions to the stratigraphic nomenclature of the Santa Fe Group, northwestern Albuquerque basin, New Mexico: *New Mexico Geological Society Guidebook*, **50**, 337–353.

Connell, S.D., 2004, Geology of the Albuquerque basin and tectonic development of the Rio Grande rift in north-central New Mexico: in Mack, G.H., and Giles, K.A., (eds.), *The Geology of New Mexico, A Geologic History*: New Mexico Geological Society, 359–388.

Grauch, V.J.S., Hudson, M.R., and Minor, S.A., 2000, Aeromagnetic signatures of intrabasinal faults, Albuquerque basin, New Mexico: Implications for layer thickness and magnetization: *70th Annual International Meeting, Society of Exploration Geophysicists, Expanded Abstracts*, 363–366.

Grauch, V.J.S., Hudson, M.R., and Minor, S.A., 2001, Aeromagnetic expression of faults that offset basin fill, Albuquerque basin, New Mexico: *Geophysics*, **66**, 707–720.

Gunn, P.J., 1997, Application of aeromagnetic surveys to sedimentary basin studies: *AGSO Journal of Australian Geology and Geophysics*, **17**, 133–144.

Hudson, M.R., Grauch, V.J.S., and Minor, S.A., 2006, *Rock magnetic characterization of faulted sediments with associated magnetic anomalies in the Albuquerque basin, Rio Grande rift, New Mexico*: preprint, 47 pp.

Hudson, M.R., Grauch, V.J.S., Minor, S.A., Caine, J.S., and Hudson, A.M., 2001, Rock magnetic properties, magnetic anomalies, and intrabasin faulting: Santa Fe Group basin fill, Rio Grande rift, New Mexico: *EOS, Transactions, American Geophysical Union*, **82**, 338–339.

Koning, D.J., Pederson, J., Pazzaglia, F.J., and Cather, S.M., 1998, Geology of the Cerro Conejo (Sky Village NE) 7.5-min. quadrangle, Sandoval County, New Mexico: *New Mexico Bureau of Mines and Mineral Resources Open-file Geologic Map OF-GM 45*, scale 1:24,000.

Mushayandebvu, M.F., and Davies, J., 2006, Magnetic gradients in sedimentary basins: Examples from the Western Canada Sedimentary Basins: *The Leading Edge*, **25**, 69–73.

Reid, A.B., 1980, Aeromagnetic survey design: *Geophysics*, **45**, 973–976.

Reid, A.B., 2003, Euler magnetic structural index of a thin-bed fault: *Geophysics*, **68**, 1255–1256.

Reid, A.B., Allsop, J.M., Granser, H., Millett, A.J., and Somerton, I.W., 1990, Magnetic interpretation in three dimensions using Euler deconvolution: *Geophysics*, **55**, 80–91.

Russell, L.R., and Snelson, S., 1994, Structure and tectonics of the Albuquerque Basin segment of the Rio Grande rift: Insights from reflection seismic data: in Keller, G.R., and Cather, S.M., (eds.), *Basins of the Rio Grande rift: Structure, stratigraphy, and tectonic setting: Geological Society of America Special Paper 291*, 83–112.

Sweeney, R.E., Grauch, V.J.S., and Phillips, J.D., 2002, Merged digital aeromagnetic data for the Albuquerque and southern Española Basins, New Mexico: *U. S. Geological Survey Open-File Report 02–205*. [Web document]: Accessed 31 October, 2006. Available at <http://pubs.usgs.gov/of/2002/ofr-02-0205/>

U. S. Geological Survey, Sander Geophysics Ltd., and Geoterrex, 1999, Digital data from the Sandoval-Santa Fe, Belen, and Cochiti aeromagnetic surveys, covering areas in Sandoval, Santa Fe, Rio Arriba, Valencia, and Socorro Counties, New Mexico: *U. S. Geological Survey Open-File Report 99-404*, CD-ROM.